New Aspects of the Hadron and Astro/Nuclear Physics
(Uzbekistan, 2018)
International Journal of Modern Physics: Conference Series
Vol. 49 (2019) 1960011 (8 pages)

DOI: 10.1142/S2010194519600115

On the fluorine nucleosynthesis in AGB stars in the light of the $^{19}F(p,\alpha)^{16}O$ and $^{19}F(\alpha,p)^{22}Ne$ reaction rate measured via THM

S. Palmerini

Dipartimento di Fisica e Geologia, Università degli Studi di Perugia, via A. Pascoli, I-06125 Perugia, Italy

I.N.F.N. Sezione di Perugia, via A. Pascoli, I-06125 Perugia, Italy
sara.palmerini@pg.infn.it

G. D'Agata

Nuclear Physics Institute of the Czech Academy of Sciences, p.r.i., Řež 130, Řež, 25068 Czech Republic

M. La Cognata, R. G. Pizzone and I. Indelicato

I.N.F.N. Laboratori Nazionali del Sud, Via Santa Sofia 62, I-95123, Catania, Italy

O. Trippella

I.N.F.N. Sezione di Perugia, via A. Pascoli, I-06125 Perugia, Italy

D. Vescovi

Gran Sasso Science Institute, Viale Francesco Crispi, 7, 67100 L'Aquila, Italy

I.N.F.N. Sezione di Perugia, via A. Pascoli, I-06125 Perugia, Italy

Published 25 July 2019

In the last years the $^{19}F(p,\alpha)^{16}O$ and the $^{19}F(\alpha,p)^{22}Ne$ reactions have been studied via the Trojan Horse Method in the energy range of interest for astrophysics. These are the first experimental data available for the main channels of ^{19}F destruction that entirely cover the energy regions typical of the stellar H- and He- burning. In both cases the reaction rates are significantly larger than the previous estimations available in the literature. We present here a re-analysis of the fluorine nucleosynthesis in Asymptotic Giant Branch stars by employing in state-of-the-art models of stellar nucleosynthesis the THM reaction rates for ^{19}F destruction.

Keywords: Nuclear reactions; nucleosynthesis; stars: AGB and post-AGB.

1. The Fluorine Problem

Is the ^{19}F synthesis in Asymptotic Giant Branch (AGB) stars sufficient to account for the whole fluorine abundance in the Galaxy? This is an open question of the nuclear astrophysics. Relatively large abundances of fluorine have been observed by several authors in the spectra of a large sample of AGB stars (see e.g. Ref. 1 and references therein) as well as the very complicate network of reactions responsible for fluorine production and destruction has been investigated by a lot of models for AGB star evolution and nucleosynthesis (see e.g. Refs. 2 and 3). However discrepancies between observations and predictions continue to exist and at least 3 other scenarios for fluorine nucleosynthesis have been suggested. Indeed also Type II supernovae (SNe II) produce fluorine via the neutrino process during the core collapse converting ^{20}Ne into ^{19}F,[4] as well as Wolf-Rayet (WR) stars produce F via a nucleosynthesis network similar to the one burned by AGB stars[5,6] and hydrogen-deficient stars formed by white-dwarf merging show high carbon and fluorine abundances by Ref. 7. Because of the number of objects belonging to each one of these three kind of stars and the amount of processed mass that they reverse into the interstellar medium, SNeII progenitors are the most likely source of ^{19}F alternative (or complementary) to AGB stars.

A good method to disentangle among the suggested nucleosynthesis sites is to compare the observed abundance of fluorine with those of elements, which are finger prints of supernovae nucleosynthesis. In particular Ref. 8 observed [F/Fe] versus [Fe/H] and [F/O] versus [O/H] trends in a sample of 49 bright K giants of the near Galaxy. Both the trends were found to increase and this fact hints that ν-process could not be the dominant fluorine producer in the solar neighborhood. At odds with the conclusion by Ref. 1, stating that state that the yields from AGB stars are not enough to account for the whole fluorine abundance in the Milky Way, the findings of Ref. 8 seems to confirm that AGB stars are the main site of fluorine production in galaxy.

Since the abundance of an element can be larger than theoretical predictions because the channels of its production are more efficient than expected or because its the destruction mechanisms are less efficient. We investigate this latter hypothesis by employing in AGB nucleosynthesis calculations the $^{19}\mathrm{F}(\alpha,\mathrm{p})^{22}\mathrm{Ne}$ and $^{19}\mathrm{F}(\mathrm{p},\alpha)^{16}\mathrm{O}$ reaction rate recently measured at astrophysical energies by the Trojan Horse Method (hereafter THM). Indeed the ^{19}F is the sole stable isotope of fluorine and it can be easily destroyed by both proton- and α-captures.

2. Fluorine Nucleosynthesis in AGB Stars

After the core He-burning phase stars with mass smaller than 6–8 $M_\odot$ climb for the second time the giant branch, undergoing the evolved phase or the Asymptotic Giant Branch (AGB). In this stage the stellar structure is made of a degenerate un-burning core (of C and O), surrounded by an shell rich in He, where episodes of convective He-burning, called thermal pulses (TP) occur periodically, a thin

radiative H-burning shell that the main source of energy for the star and a cold extended convective envelope. The ignition of each TP interrupts the H-burning and at the end of each pulse the convective envelope penetrates into the inner stellar region bringing into the surface the fresh product of the stellar nucleosynthesis, this phenomenon is known as *third dredge-up* (hereafter, TDU).

AGB stars are important sites for the production of nuclei heavier than Fe by the slow neutron capture nucleosynthesis (or *s*-process), which occurs in the He-shell during the TPs as well as during the H-burning phase (in the upper layers of the He-shell often called inter-shell). In this latter scenario neutrons are released by the $^{13}C(\alpha, n)^{16}O$ reaction and the formation of a ^{13}C reservoir in this stellar region is crucial for the s-process. We briefly summarise decades of studies about on the ^{13}*C-pocket* formation reminding that it is due to an injection of protons in the He-intershell during the TDU that triggers the reaction chain $^{12}C(p, \gamma)^{13}N(\beta)^{13}C$, being the ^{12}C the second most abundant nucleus in the He-shell. If the injected protons are enough ^{14}N is produced too, by further proton captures on ^{13}C.

Even if the production of ^{14}N has to be avoided to guarantee an efficient s-process nucleosynthesis, because of the large neutron capture cross section of the isotope, ^{14}N is the seed of the ^{19}F production through the chain $^{14}N(\alpha, \gamma)^{18}F(\beta^+\nu)^{18}O(p, \alpha)^{15}N(\alpha, \gamma)^{19}F$ or, alternatively, $^{18}O(p, \alpha)^{15}N(\alpha, \gamma)^{19}F$ if enough protons are released by the $^{14}N(n, p)^{14}C$ reaction.[9,10] Part of the ^{19}F then undergoes α-captures when the materials of the He-shell are engulfed in a TP (at $T \geq 2.5 \cdot 10^8\, K$). Indeed the $^{19}F(\alpha, p)^{22}Ne$ reaction is the main channel for fluorine destruction in AGB stars. If unburned ^{13}C is still available a further production of ^{19}F might occur via the $^{15}N(\alpha, \gamma)^{19}F$ reaction, but this rare possibility is not be analyzed in this work.

The temperature of H-burning in AGB stars is not high enough to allow the production of ^{19}F via proton capture on ^{16}O, but it is sufficient to burn ^{19}F via the $^{19}F(p, \alpha)^{16}O$ and the $^{19}F(p, \gamma)^{20}Ne$ reactions (being the first the most efficient one). Furthermore, at a few $10^7\, K$ proton captures coupled with non convective exchanging of matter between the border of the convective envelope and the H-burning shell (called extra-mixing[11]) can contribute to reduce the surface abundance of fluorine in AGBs of mass smaller than $3\, M_\odot$.[12]

Figure 1 reports a scheme of the temporal evolution of the internal structure of an AGB star and underlines the sites where the reactions belonging to the complicate network of ^{19} nucleosynthesis take place.

3. Study of the $^{19}F(p, \alpha)^{16}O$ and the $^{19}F(\alpha, p)^{22}Ne$ Reactions via the Trojan Horse Method

The first experimental data available in literature for the $^{19}F(p, \alpha)^{16}O$ at astrophysical energies ($E_{c.m.} \leq 300\,keV$) were published by Ref. 13, which investigated the energy region where fluorine burning is most effective thanks to the THM (Trojan Horse Method). Indeed this indirect technique allows to measure a two body

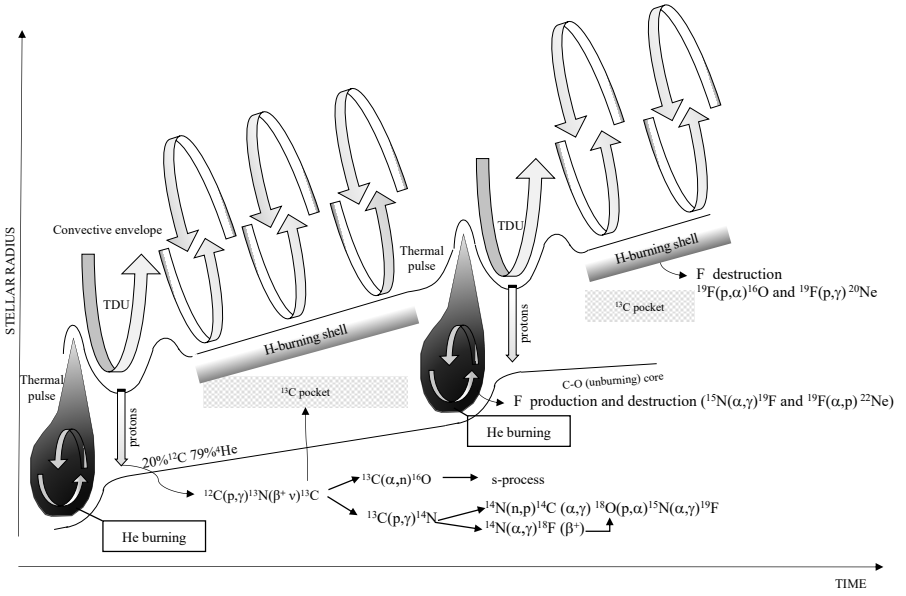

Fig. 1. Scheme of the evolution of the internal structure of an AGB star. The "drop" structures are thermal pulses. The arrows indicate the stellar regions where the the nucleosynthesis reactions take place. The labels show the H-burning shell, the He-shell, the ^{13}C-pocket and the convective envelop.

reaction (having two massive particle in the exit channel) down to the Gamow-peak energy region by performing a three-body reaction at a beam energy high enough to overcome the Coulomb barrier in the reaction entrance channel (for more detail see Ref. 14, and references therein). In particular the cross-section of the two-body $^{19}\mathrm{F}(\mathrm{p},\alpha)^{16}\mathrm{O}$ has been determined applying the THM to the three-body reaction $^{2}\mathrm{H}(^{19}\mathrm{F},\alpha^{16}\mathrm{O})\mathrm{n}$, where n plays the role of the spectator particle and ^{2}H acts as the TH nucleus because of its $\mathrm{p}\oplus\mathrm{n}$ cluster structure. The first measurement by Ref. 13 hinted to the presence of resonant structures at $\mathrm{E_{cm}} \leq 0.6\,\mathrm{MeV}$ and a consequent enhancement of the reaction rate at astrophysical temperatures (about 10^{7}–$10^{8}\,K$). Other two THM experiments were performed Refs. 12, 15, the results confirmed the previous findings and in particular the S(E) factors extracted from the most recent experiment[15] is larger because of a resonance at 251 keV (at $\mathrm{E_{cm}} \leq 0.6\,\mathrm{MeV}$), which had not been observed before.[12,13] From R-matrix calculation it turns out that the difference among the reaction rates ([12,15]) are small ($\sim 10\%$) at $\mathrm{T_9} = 0.04$–0.2, while larger discrepancy ($\sim 30\%$) is found at a temperature $\mathrm{T_9} \geq 0.04$. In any case an enhancement of the reaction rate at at $\mathrm{E_{cm}} \leq 0.6\,\mathrm{MeV}$ is also confirmed by the direct data extracted from Ref. 18. Comparisons of the $^{19}\mathrm{F}(\mathrm{p},\alpha)^{16}\mathrm{O}$ reaction rates estimated by the THM and the one already present in literature[19] are reported by Ref. 15 (Figs. 13–16 in particular) along with a detailed discussion on the data analysis and on the results.

The $^{19}\mathrm{F}(\alpha,\mathrm{p})^{22}\mathrm{Ne}$ reaction has also been investigated successfully via the THM. In this cases direct studies in the energy range typical of stellar He-burning (200–1100 keV) are hampered by the Coulomb barrier at about 3.1 MeV. Indeed the lowest energy at which the reaction has been directly measured is 660 keV[17] and in any case data available in literature are affected by large uncertainties. The $^{19}\mathrm{F}(^{6}\mathrm{Li},\mathrm{p}^{22}\mathrm{Ne})^{2}\mathrm{H}$ reaction was chosen to to investigate the $^{19}\mathrm{F}(\alpha,\mathrm{p})^{22}\mathrm{Ne}$ via the THM because of the well-known cluster structure of the ^{6}Li nucleus ($\alpha \oplus d$), which under proper kinematical conditions allows the deuteron to plays as a spectator nucleus. Two papers report the results about the study of the $^{19}\mathrm{F}(\alpha,\mathrm{p})^{22}\mathrm{Ne}$ via the THM, Refs. 20 and 16, and both agrees in stating that the $^{19}\mathrm{F}(\alpha,\mathrm{p})^{22}\mathrm{Ne}$ reaction rate is up to a factor of 4 larger than what estimated trough direct measurements (Ref. 17 and references there in) in the energy region of stellar nucleosynthesis. Such an enhancement is shown by Fig. 2(a) and in Table 4 of Ref. 16.

3.1. *Results for fluorine nucleosynthesis in AGB stars*

We performed our study of the implications of the THM reaction rate to fluorine nucleosynthesis in AGB stars in two steps. Firstly we analysed the effects of the $^{19}\mathrm{F}(\alpha,\mathrm{p})^{22}\mathrm{Ne}$ rate and later the ones of the $^{19}\mathrm{F}(\mathrm{p},\alpha)^{16}\mathrm{O}$. In doing that calculations for fluorine production/destruction in the He-rich stellar layers (during both the H-burning periods and the TPs) of three stellar models of 1.5, 3, and 5 $M_{\odot}$ and solar metallicity were performed by the NEWTON code.[21] The output obtained by using the $^{19}\mathrm{F}(\mathrm{p},\alpha)^{16}\mathrm{O}$ reaction rate by Ref. 17 were compared with those obtained by having in input the THM rate. To better appreciate the effects of the α-capture reaction rate, phenomena of ^{19}F destruction due to proton captures, such as the

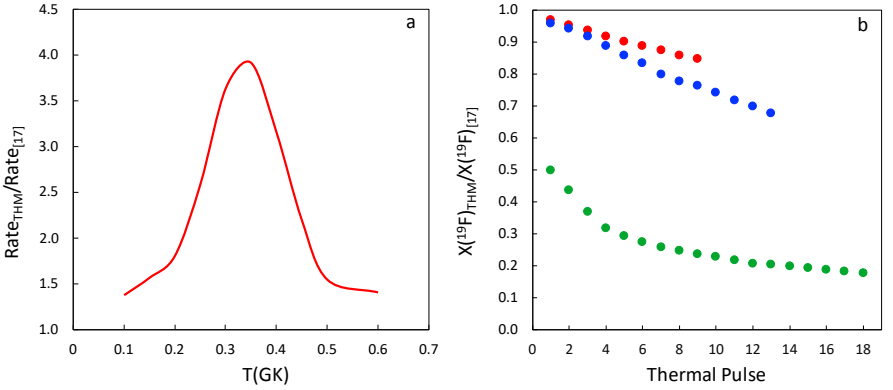

Fig. 2. Panel (a). Ratio between the value of the $^{19}\mathrm{F}(\alpha,\mathrm{p})^{22}\mathrm{Ne}$ rate extracted by the THM, and recommended by Ref. 16, and the one recommended by Ref. 17, as a function of the temperature in units of 10^9 K. Panel (b). Ratio between the ^{19}F abundance in the He-shell calculated by using the $^{19}\mathrm{F}(\alpha,\mathrm{p})^{22}\mathrm{Ne}$ reaction rate determined via THM and the prediction computed by employing the reaction rate of Ref. 17. The ratio is reported as a function of the TP, namely as a function of the time. Red, blue and green dots refer to AGB models of 1.5, 3, and 5 $M_{\odot}$, respectively.

extra-mixing (Ref. 11 and references therein) and hot bottom burning (in the case of the $5\,M_{\odot}$ model[22]) were not considered in this step of our analysis. We used the reaction rates of proton- and α- captures reported in Table 5 by Ref. 16, the same cross-sections for neutron-capture reactions used by the quoted authors and the mechanism of ^{13}C-pocket formation suggested by Refs. 23 and 24. We underline this last detail because of the sensitivity of resulting pockets of ^{13}C and ^{14}N to the profile of the proton injection in the inter-shell at the moment of the TDU.

Figure 2(b) shows the ratios between the ^{19}F abundance profile in the He-shell predicted by adopting the THM $^{19}\mathrm{F}(\alpha,\mathrm{p})^{22}\mathrm{Ne}$ reaction rate and the one calculated by using the rate by Ref. 17. The red, the blue and the green curve refer to AGB models of 1.5, 3, and $5\,M_{\odot}$, respectively. At the typical temperature of the He-shell burning, the THM rate is always larger than the one by Ref. 17, as illustrated by Fig. 2(a). Therefore, tt turns out that ^{19}F is more easily destroyed during TP and its abundances in the He-shell are smaller.

At $3.6 \cdot 10^8\,K$ the difference between the THM cross-section for $^{19}\mathrm{F}(\alpha,\mathrm{p})^{22}\mathrm{Ne}$ and the Ref. 17 one is maximum. Since this is the temperature reached during the He-burning in our $5\,M_{\odot}$ model it is the most sensitive to the reaction rate used in calculations. Smaller variations are instead registered in the 1.5 and $3\,M_{\odot}$ models, where temperatures in the He-shell are lower.

Each TDU brings into the stellar envelope part of the ashes of the He-burning. In this way the nucleosynthesis products are diluted with envelope materials and the effects of the $^{19}\mathrm{F}(\alpha,\mathrm{p})^{22}\mathrm{Ne}$ reaction rate become negligible. Indeed, none of the studied cases shows a variation of the abundance of fluorine larger than 5% due to the choice of the input for the $^{19}\mathrm{F}+\alpha$ reaction. A discussion on the implication on AGB nucleosynthesis of employing in calculations lower and upper limits of the reaction rate is reported by Ref. 16.

In the second step of our analysis the destruction of fluorine due to the $^{19}\mathrm{F}(\mathrm{p},\alpha)^{16}\mathrm{O}$ reaction in the H-shell was studied. The composition of the H-burning shell of a $2\,M_{\odot}$ and solar metallicity AGB star was computed by the SHELL nucleosynthesis code.[11,25] Figure 3(a) illustrates the three profile of the ^{19}F abundance obtained by using the $^{19}\mathrm{F}+\mathrm{p}$ rates published by Refs. 12, 15 and 19, respectively. As expected the models that employ a larger reaction rate are the ones showing smaller fluorine abundances. Furthermore, the MAGIC post-process code[11,25] was run to estimate the effects on the F abundance in the stellar envelope of extra-mixing phenomena[a] in the light of the three rates of the $^{19}\mathrm{F}(\mathrm{p},\alpha)^{16}\mathrm{O}$ reaction (Refs. 12, 15 and 19). Figure 3(b) shows the results: ^{19}F abundance profiles in the envelope of our $2\,M_{\odot}$ AGB model are drawn as a function of the time, from the beginning of the AGB phase. Finally, in Fig. 3(c) the predictions of our models are compared with the F abundance observed by Ref. 1 in a sample of AGB stars. The three models are all in a quite good agreement with the observations and the choice made for the $^{19}\mathrm{F}(\mathrm{p},\alpha)^{16}$ cross section has almost a negligible effects . We decided to do

[a]The extra-mixing model we use is the one described in Ref. 26.

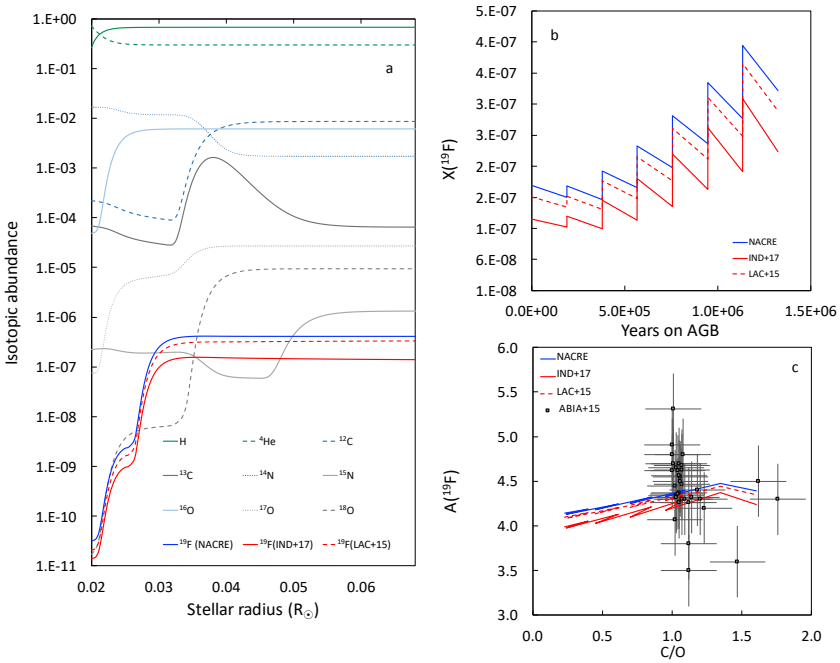

Fig. 3. Panel (a). Isotopic composition of the H-shell of our $2\,M_{\odot}$ and solar metallicity AGB model. Abundances of isotopes involved in H-burning and of ^{19}F are shown as a function of the stellar radius. Three curves deal with the fluorine abundance profile computed by using the $^{19}\mathrm{F}(\mathrm{p},\alpha)^{16}\mathrm{O}$ reaction rate by Ref. 19 (blue line), Ref. 12 (red dashed line) and Ref. 15 (red solid line). Panel (b). Temporal evolution of the ^{19}F abundance in the envelope of the $2\,M_{\odot}$ and solar metallicity AGB model. The step wise trend is due to the enrichment in F at each TDU (which brings into the envelope the ashes of the He-burning) and the F destruction of the extra-mixing during the H-burning periods. The three curves show the model outputs obtained with the three $^{19}\mathrm{F}(\mathrm{p},\alpha)^{16}\mathrm{O}$ reaction rates we are studying. Panel (c). Comparison between the predictions of our stellar model for the ^{19}F surface abundance and the observed ones in a sample of AGBs by Ref. 1. The F abundances are given using the definition $\mathrm{A}(^{19}\mathrm{F}) = 12 + \log(\mathrm{X}(^{19}\mathrm{F})/\mathrm{H})$, being $\mathrm{X}(^{19}\mathrm{F})$ the abundance of ^{19}F by number, and are reported as a function of the C/O ratio.

not report the output of the models run by using upper and lower limits of the 3 $^{19}\mathrm{F}(\mathrm{p},\alpha)^{16}\mathrm{O}$ reaction rates because we found that the nucleosynthesis predictions agree the one with the other. Moreover it is evident (in particular from the panel (c) of Fig. 3) that the major uncertainties are those raise from the stellar observations.

References

1. C. Abia, K. Cunha, S. Cristallo *et al.*, *A&A* **581**, 88 (2015).
2. M. Lugaro, C. Ugalde, A. I. Karakas *et al.*, *ApJ* **615**, 934 (2004).
3. S. Cristallo, A. Di Leva, G. Imbriani *et al.*, *A&A* **570**, 46 (2014).
4. S. E. Woosley and W. C. Haxton, *Nature* **334**, 45 (1998).
5. G. Meynet and M. Arnould, *A&A* **355**, 176 (2000).
6. A. Palacios, M. Arnould and G. Meynet, *A&A* **443**, 243 (2005).
7. R. Longland, P. Lorén-Aguilar, J. José *et al.*, *ApJL* **737**, 34 (2011).

8. H. Jönsson, N. Ryde, E. Spitoni *et al.*, *ApJ* **835**, 50 (2017).
9. S. Cristallo, O. Straniero, R. Gallino *et al.*, *ApJ* **696**, 797 (2009).
10. M. Forestini, S. Goriely, A. Jorissen and M. Arnould, *A&A* **261**, 157 (1992).
11. S. Palmerini, M. La Cognata, S. Cristallo and M. Busso, *ApJ* **729**, 3 (2011).
12. M. La Cognata, S. Palmerini, C. Spitaleri *et al.*, *ApJ* **805**, 128 (2015).
13. M. La Cognata, A. M. Mukhamedzhanov, C. Spitaleri *et al.*, *ApJL* **739**, 54 (2011).
14. C. Spitaleri, M. La Cognata, L. Lamia *et al.*, *EPJA* **52**, 77 (2016).
15. I. Indelicato, M. La Cognata, C. Spitaler *et al.*, *ApJ* **845**, 19 (2017).
16. G. D'Agata, R. G. Pizzone, M. La Cognata *et al.*, *ApJ* **860**, 61 (2018).
17. C. Ugalde, R. E. Azuma, A. Couture *et al.*, *PhRvC* **77**, 035801 (2008).
18. I. Lombardo, D. Dell'Aquila, A. Di Leva *et al.*, *PhLB* **748**, 178 (2015).
19. C. Angulo, M. Arnould, M. Rayet *et al.*, *NuPhA* **656**, 3 (1999).
20. R. G. Pizzone, G. D'Agata, M. La Cognata *et al.*, *ApJ* **836**, 57 (2017).
21. O. Trippella, M. Busso, E. Maiorca *et al.*, *ApJ* **787**, 41 (2014).
22. I. J. Sackmann and A. I. Boothroyd, *ApJL* **392**, 71 (1992).
23. O. Trippella, M. Busso, S. Palmerini *et al.*, *ApJ* **818**, 125 (2016).
24. S. Palmerini, O. Trippella, M. Busso *et al.*, *Ge.Co.A.* **221**, 21 (2018).
25. S. Palmerini, S. Cristallo, M. Busso *et al.*, *ApJ* **741**, 26 (2011).
26. S. Palmerini, O. Trippella and M. Busso, *MNRAS* **467**, 1193 (2017).